FACTA UNIVERSITATIS
Series: **Physics, Chemistry and Technology** Vol. 17, N° 2, 2019, pp. 131 - 144
https://doi.org/10.2298/FUPCT1902131P

ELECTROMAGNETICALLY INDUCED TRANSPARENCY IN A RECTANGULAR QUANTUM DOT ON A SINGLE ELECTRON[†]

UDC 535.337

Vladan Pavlović, Željko Laić, Ljiljana Stevanović, Nikola Filipović

Department of Physics, Faculty of Sciences and Mathematics, University of Niš, Niš, Serbia

Abstract. *In this paper, we investigated the realization of electromagnetically induced transparency (EIT) in a rectangular quantum dot (QD) with a single electron in the presence of probe and control laser fields. The lowest three levels of the confined electron that form ladder and V configuration were chosen. We discussed the dependence of density matrix elements ρ_{21} for ladder configuration and ρ_{31} for V configuration on detunings of the probe field for various values of quantum dot dimensions. This dependence is discussed for both cases, at cryogenic temperatures when spontaneous emission dominates the relaxation mechanism and at room or higher temperatures when dephasing rate cannot be neglected.*

Key words: *Electromagnetically induced transparency, Quantum dot, Ladder configuration, V configuration*

1. INTRODUCTION

Electromagnetically induced transparency (EIT) is an example of the coherent interaction of laser fields and a medium (multi-level atoms) which is characterized by the appearance of a transparency window in the absorption spectrum (Pavlović et al., 2016). The phenomenon of EIT typically involves a three-level system, having two dipole-allowed transitions and the third dipole forbidden transition. Driving this system with a control field of resonant angular frequency ω_c and probe field of resonant angular frequency ω_p establishes the coherent superposition of the probability amplitudes and makes quantum interference possible. Using EIT we can achieve that the light beam which was at first completely absorbed by an opaque medium, can go through just by shining that medium by another light beam of a certain wavelength (Kasapi et al., 1995). EIT is also closely related to the change of refraction index in a way it becomes

Received February 26th, 2019; accepted October 16th, 2019
[†] Acknowledgement: The authors would like to thank the Ministry of Science, Education and Technological Development of the Republic of Serbia for funding this research under the projects OI171025, OI171028 and III45010.
Corresponding author: Vladan Pavlović, Department of Physics, Faculty of Sciences and Mathematics, University of Niš, Višegradska 33, 18000 Niš • E-mail: vladan.pavlovic@pmf.edu.rs

significantly larger for certain wavelengths. Since the group velocity is determined by the refraction index, this effect can be used for reducing the speed of light up to seven orders of magnitude, i.e. to 90 m/s (Kash et al., 1999), 17 m/s (Hau et al., 1999), and 8 m/s (Budker et al., 1999), or to completely stop light (Liu et al., 2001).

The phenomenon of EIT was first predicted by the work of Arkhipkin and Heller in 1983 (Arkhipkin et al., 1983) and further elucidated and improved by theoretical work of S.E. Harris (Harris, 1989).

An experimental realization of the effect was demonstrated by K. J. Boller, A. Imamoglu, and S. E. Harris in strontium vapor (Boller et al., 1991).

There has been an intensive investigation of quantum coherence effects in semiconductor nanostructures like quantum dots. A growing interest in this field of research also comes from the potential applications of nanocrystals in electronic and optoelectronic devices, quantum computing and quantum information processing (Beausoleil et al., 2004).

In this paper, we discussed the theoretical model for the realization of EIT in GaAs rectangular quantum dot with a single electron. The theoretical model which is presented includes: master equations with their solution in a case of a steady-state regime for ladder and *V* configuration, analytically obtained eigenenergies and eigenstates for a particle in a QD and the dependence of real and imaginary part of matrix elements of interest (ρ_{21} and ρ_{31}) on probe field detunings for different quantum dot dimensions at cryogenic and room temperatures.

1.THEORY

In order to understand the physics behind EIT, we adopt a quantum mechanical approach to analyze a three-level system described by Hamiltonian H_0. Eigenstates of this system are designated as $|1\rangle$, $|2\rangle$ and $|3\rangle$ with corresponding eigenenergies E_1, E_2 and E_3 (where $E_1 < E_2 < E_3$). The system is coupled by two near-resonance electromagnetic fields, commonly called *control and probe*, which are assumed to be monochromatic so they can be described by:

$$\boldsymbol{\mathcal{E}_c} = \frac{1}{2}(\boldsymbol{E_c} e^{-i\omega_c t} + \boldsymbol{E_c^*} e^{i\omega_c t}), \tag{1}$$

$$\boldsymbol{\mathcal{E}_p} = \frac{1}{2}\left(\boldsymbol{E_p} e^{-i\omega_p t} + \boldsymbol{E_p^*} e^{i\omega_p t}\right), \tag{2}$$

where E_c and E_p contain the information concerning the polarization and amplitude while ω_c and ω_p are angular frequencies of corresponding fields.

Two types of configurations that can be formed in a three-level system will be discussed in detail. The first one, typically called *ladder* or *cascade* is formed when probe and control laser fields induce transitions $|1\rangle \leftrightarrow |2\rangle$ and $|2\rangle \leftrightarrow |3\rangle$, respectively. The second one is named *V* configuration (due to its shape), and it is formed when the control laser induces the transition $|1\rangle \leftrightarrow |2\rangle$ and the probe laser induces the transition $|1\rangle \leftrightarrow |3\rangle$. See Fig. 1.

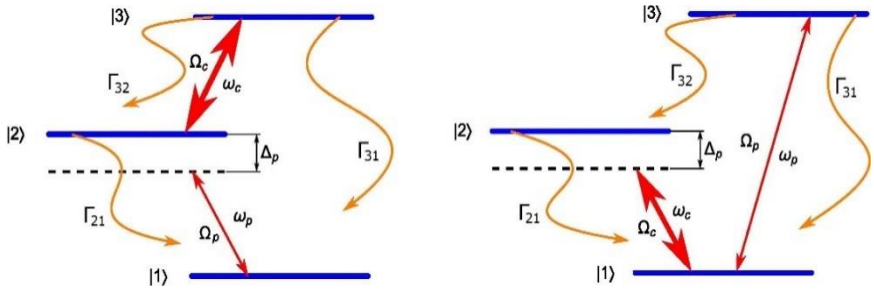

Fig. 1 Scheme of the levels and fields in ladder and *V* configuration

We shall also introduce the frequencies of transitions we consider: $\omega_{32} = (E_3 - E_2)/\hbar$ and $\omega_{21} = (E_2 - E_1)/\hbar$. As the consequence of the existence of the spontaneous emission we associate certain decay coefficients for each transition: Γ_{21}, Γ_{32} and Γ_{31} to describe the spontaneous emission associated with the spontaneous decays $|2\rangle \leftrightarrow |1\rangle$, $|3\rangle \leftrightarrow |2\rangle$ and $|3\rangle \leftrightarrow |1\rangle$, respectively.

2.1. Ladder configuration

Due to the presence of the probe and control fields, we need to change the Hamiltonian of the atomic system H_0, such that the Hamiltonian H_I describing the interaction between the system and the incoming fields has to be added:

$$H = H_0 + H_I. \tag{3}$$

Hamiltonian H_I can be written as:

$$\mathrm{H_I} = -\mathrm{d}(\boldsymbol{\mathcal{E}}_c + \boldsymbol{\mathcal{E}}_p), \tag{4}$$

where $\mathbf{d} = -\mathrm{e}\mathbf{r}$ is the transition dipole moment operator and for the transition of an electron from state $|i\rangle$ to $|j\rangle$ it is calculated as follows:

$$\mathbf{d_{ij}} = -e\langle i|\mathbf{r}|j\rangle. \tag{5}$$

Thus, eigenstates of H_0 ($|1\rangle$, $|2\rangle$ and $|3\rangle$) are in general no longer eigenfunctions of H. Using the rotating wave approximation and dipole approximation one can find that the new Hamiltonian for the ladder configuration is given by (Bing et al., 2011):

$$H_{\Xi} = \hbar \begin{pmatrix} 0 & -\Omega_p^* & 0 \\ -\Omega_p & \Delta_p & -\Omega_c^* \\ 0 & -\Omega_c & \Delta_p + \Delta_c \end{pmatrix}. \tag{6}$$

Here we introduced Ω_p and Ω_c, quantities known as *Rabi frequencies*, which are for ladder configuration defined as follows:

$$\Omega_p = \frac{\boldsymbol{d_{21}E_p}}{2\hbar}, \tag{7}$$

$$\Omega_c = \frac{\boldsymbol{d_{31}E_c}}{2\hbar}, \tag{8}$$

and frequency detunings: $\Delta_\mathrm{p} = \omega_{21} - \omega_\mathrm{p}$ and $\Delta_\mathrm{c} = \omega_{32} - \omega_\mathrm{c}$. The evolution of elements of *density matrix* ρ can be found from the modified Liouville equations:

$$\dot{\rho}_{\mathrm{nn}} = -\frac{i}{\hbar}[H_\Xi, \rho]_{nn} + \sum_{E_>E_n} \Gamma_{nm}\,\rho_{mm} - \sum_{E_m<E_n} \Gamma_{mn}\,\rho_{nn}, \tag{9}$$

$$\dot{\rho}_{\mathrm{mn}} = -\frac{i}{\hbar}[H_\Xi, \rho]_{mn} - \gamma_{mn}\rho_{mn}, \tag{10}$$

where the first equation is used for diagonal and the second for non-diagonal elements. Coefficients Γ_{ij} denote the population decay rate from the state $|i\rangle$ to state $|j\rangle$ while $\gamma_{13} = \frac{1}{2}(\Gamma_{31} + \Gamma_{32}) + \Gamma_{13}^{dph}$, $\gamma_{12} = \frac{1}{2}\Gamma_{21} + \Gamma_{12}^{dph}$ and $\gamma_{23} = \frac{1}{2}(\Gamma_{32} + \Gamma_{31} + \Gamma_{21}) + \Gamma_{23}^{\mathrm{dph}}$ are the relaxation rates of the corresponding coherences. Coefficients $\Gamma_{\mathrm{ij}}^{\mathrm{dph}}$ $(i \neq j)$ represent the dephasing rate of the quantum coherence of the $|i\rangle \leftrightarrow |\mathrm{j}\rangle$ transition. These dephasing rates originate from the electron-phonon interactions.

Taking into account that $\rho_{11} + \rho_{22} + \rho_{33} = 1$ and $\rho_{ij} = \rho_{ji}^*$, we conclude that the density matrix is fully specified only by five elements. Thus, it is enough to solve the system of five differential equations in order to find all density matrix elements. We choose to write master equations for elements $\rho_{11}, \rho_{22}, \rho_{12}, \rho_{13}$ and ρ_{23}. Since the Hamiltonian is given by (6), master equations for these elements take the form (Wang, 2009):

$$\dot{\rho}_{11} = \mathrm{i}\Omega_p^*\rho_{21} - \mathrm{i}\Omega_p\rho_{12} + \Gamma_{21}\rho_{22} + \Gamma_{31}\rho_{33}, \tag{11}$$

$$\dot{\rho}_{33} = i\Omega_c\rho_{23} - i\Omega_c^*\rho_{32} - \Gamma_{32}\rho_{33} - \Gamma_{31}\rho_{33}, \tag{12}$$

$$\dot{\rho}_{12} = \mathrm{i}\Omega_p^*(\rho_{22} - \rho_{11}) - \mathrm{i}\Omega_c\rho_{13} + \big(i\Delta_p - \gamma_{12}\big)\rho_{12}, \tag{13}$$

$$\dot{\rho_{13}} = i\Omega_p^*\rho_{23} - i\Omega_c^*\rho_{12} + \big[i\big(\Delta_p + \Delta_c\big) - \gamma_{13}\big]\rho_{13}, \tag{14}$$

$$\dot{\rho_{23}} = i\Omega_c^*(\rho_{33} - \rho_{22}) + i\Omega_p\rho_{13} + (i\Delta_c - \gamma_{23})\rho_{23}. \tag{15}$$

Assuming that the control field is much stronger than the probe field, the latter can be treated as a perturbation and written down as $\Omega_p = \lambda\Omega_p$. The iterative method is used and the density matrix elements are expressed as $\rho_{ij} = \sum_{k=0}\lambda^k\rho_{ij}^{\{k\}}$. Following recursive equations are obtained in the case of a steady-state regime:

$$i\Omega_p^*\rho_{21}^{(n)} - i\Omega_p\rho_{12}^{(n)} + \Gamma_{21}\rho_{22}^{(n+1)} + \Gamma_{31}\rho_{33}^{(n+1)} = 0, \tag{16}$$

$$i\Omega_c\rho_{23}^{(n+1)} - i\Omega_c^*\rho_{32}^{(n+1)} - \Gamma_{32}\rho_{33}^{(n+1)} - \Gamma_{31}\rho_{33}^{(n+1)} = 0, \tag{17}$$

$$i\Omega_p^*\big(\rho_{11}^{(n)} - \rho_{22}^{(n)}\big) - i\Omega_c^*\rho_{13}^{(n+1)} + \big(i\Delta_p - \gamma_{12}\big)\rho_{12}^{(n+1)} = 0, \tag{18}$$

$$i\Omega_p^*\rho_{23}^{(n)} - i\Omega_c^*\rho_{12}^{(n+1)} + \big[i\big(\Delta_p + \Delta_c\big) - \gamma_{13}\big]\rho_{13}^{(n+1)} = 0, \tag{19}$$

$$i\Omega_c^*\big(\rho_{33}^{(n+1)} - \rho_{22}^{(n+1)}\big) + i\Omega_p\rho_{13}^{(n)} + [i\Delta_c - \gamma_{23}]\rho_{23}^{(n+1)} = 0. \tag{20}$$

Assuming that Rabi frequencies are real and solving this system of linear equations in terms of $\rho_{11}^{(n+1)}, \rho_{22}^{(n+1)}, \rho_{12}^{(n+1)}, \rho_{13}^{(n+1)}$ and $\rho_{23}^{(n+1)}$ we obtain:

$$\rho_{11}^{(n+1)} = \frac{2\Omega_p\left[C_2 \mathrm{Im}\rho_{12}^{(n)} + F_1^{(n)}\Omega_c(\Gamma_{12}-\Gamma_{13})\right]}{C_2\Gamma_{12}}, \tag{21}$$

$$\rho_{22}^{(n+1)} = -\frac{2\Omega_p\left[C_2 \mathrm{Im}\rho_{12}^{(n)} - F_1^{(n)}\Gamma_{13}\Omega_c\right]}{C_2\Gamma_{12}}, \tag{22}$$

$$\rho_{12}^{(n+1)} = \frac{i\Omega_p\left[C_1\left(\rho_{11}^{(n)}-\rho_{22}^{(n)}\right) - i\Omega_c\rho_{23}^{(n)}\right]}{C_1\left(i\Delta_p-\gamma_{12}\right)+\Omega_c^2}, \tag{23}$$

$$\rho_{13}^{(n+1)} = -\frac{\Omega_p\left[\Omega_c\left(\rho_{22}^{(n)}-\rho_{11}^{(n)}\right)+\rho_{23}^{(n)}\left(\Delta_p+i\gamma_{12}\right)\right]}{\Delta_p^2+\Delta_p(\Delta_c+i\gamma_{12}+i\gamma_{13})-\Omega_c^2+\gamma_{12}(i\Delta_c-\gamma_{13})}, \tag{24}$$

$$\rho_{23}^{(n+1)} = \frac{i\Omega_p\left[C_2\left(\Gamma_{12}\rho_{13}^{(n)}+2\Omega_c\mathrm{Im}\rho_{12}^{(n)}\right)-2F_1^{(n)}\Omega_c^2(\Gamma_{12}+\Gamma_{13})\right]}{C_2\Gamma_{12}(\gamma_{23}-i\Delta_c)}, \tag{25}$$

where:

$$C_1 = i\left(\Delta_c+\Delta_p\right)-\gamma_{13}, \tag{26}$$

$$C_2 = \Gamma_{12}(\Delta_c^2+\gamma_{23}^2)(\Gamma_{13}+\Gamma_{23})+2\Omega_c^2\gamma_{23}(\Gamma_{12}+\Gamma_{13}) \tag{27}$$

$$F_1^{(n)} = \gamma_{23}\left(\Gamma_{12}\mathrm{Re}\rho_{13}^{(n)}+2\Omega_c\mathrm{Im}\rho_{12}^{(n)}\right)-\Delta_c\Gamma_{12}\mathrm{Im}\rho_{13}^{(n)} \tag{28}$$

Using the system (21)) - ((25) we can find the sum $\rho_{ij} = \sum_{k=0}\lambda\rho_{ij}^{\{k\}}$ if initial values for density matrix, elements ($\rho_{11}^{(0)}, \rho_{33}^{(0)}, \rho_{13}^{(0)}, \rho_{12}^{(0)}$ and $\rho_{23}^{(0)}$) are given.

2.2. V configuration

Using the analog procedure as in the case of the ladder configuration, it can be shown that the interaction Hamiltonian operator for *V* configuration is given by (Mirzaei et al., 2014):

$$H_V = \hbar\begin{pmatrix} 0 & -\Omega_c^* & -\Omega_p^* \\ -\Omega_c & \Delta_c & 0 \\ -\Omega_p & 0 & \Delta_p \end{pmatrix}, \tag{29}$$

where Rabi frequencies for *V* configuration are given by: $\Omega_p = \frac{\boldsymbol{E_p d_{31}}}{2\hbar}$ and $\Omega_c = \frac{\boldsymbol{E_c d_{21}}}{2\hbar}$, while frequency detunings now take the form: $\Delta_p = \omega_p - \omega_{31}$ and $\Delta_c = \omega_c - \omega_{21}$. Corresponding master equations for *V* configuration can be found using (9) and (10). Thus, we obtain:

$$\dot{\rho}_{22} = i\Omega_c\rho_{12} - i\Omega_c^*\rho_{21} - \Gamma_{21}\rho_{22} + \Gamma_{32}\rho_{33}, \tag{30}$$

$$\dot{\rho}_{33} = i\left(\Omega_p\rho_{13} - \Omega_p^*\rho_{31}\right) - \Gamma_{31}\rho_{33} - \Gamma_{32}\rho_{33}, \tag{31}$$

$$\dot{\rho}_{12} = i\Omega_c^*(\rho_{22}-\rho_{11}) + \rho_{12}(i\Delta_c-\gamma_{12}) + i\Omega_p^*\rho_{32}, \tag{32}$$

$$\dot{\rho}_{13} = i\Omega_p^*(\rho_{33}-\rho_{11}) + \rho_{13}\left(i\Delta_p-\gamma_{13}\right) + i\Omega_c^*\rho_{23}, \tag{33}$$

$$\dot{\rho}_{23} = \rho_{23}\left[i\left(\Delta_p-\Delta_c\right)-\gamma_{23}\right] + i\left(\Omega_c\rho_{13}-\Omega_p^*\rho_{21}\right). \tag{34}$$

Using the same assumptions that the control field is much stronger than the probe field, following recursive equations for *V* configuration are obtained:

$$i\Omega_c\rho_{12}^{(n+1)}-i\Omega_c^*\rho_{21}^{(n+1)}-\Gamma_{21}\rho_{22}^{(n+1)}+\Gamma_{32}\rho_{33}^{(n+1)}=0, \tag{35}$$

$$i\left(\Omega_p\rho_{13}^{(n)}-\Omega_p^*\rho_{31}^{(n)}\right)-\Gamma_{31}\rho_{33}^{(n+1)}-\Gamma_{32}\rho_{33}^{(n+1)}=0, \tag{36}$$

$$i\Omega_c^*\left(\rho_{22}^{(n+1)}-\rho_{11}^{(n+1)}\right)+\rho_{12}^{(n+1)}(i\Delta_c-\gamma_{12})+i\Omega_p^*\rho_{32}^{(n)}=0, \tag{37}$$

$$i\Omega_p^*\left(\rho_{33}^{(n)}-\rho_{11}^{(n)}\right)+\rho_{13}^{(n+1)}\left(i\Delta_p-\gamma_{13}\right)+i\Omega_c^*\rho_{23}^{(n+1)}=0, \tag{38}$$

$$\rho_{23}^{(n+1)}\left[i\left(\Delta_p-\Delta_c\right)-\gamma_{23}\right]+i\left(\Omega_c\rho_{13}^{(n+1)}-\Omega_p^*\rho_{21}^{(n)}\right)=0. \tag{39}$$

Now, solving this system in terms of $\rho_{22}^{(n+1)}, \rho_{33}^{(n+1)}, \rho_{12}^{(n+1)}, \rho_{13}^{(n+1)}$ and $\rho_{23}^{(n+1)}$ we obtain:

$$\rho_{22}^{(n+1)}=\frac{\Omega_p\left(\Omega_c\Gamma F_2^{(n)}-2D_3\mathrm{Im}\rho_{13}^{(n)}\right)}{D_2\Gamma}, \tag{40}$$

$$\rho_{33}^{(n+1)}=-\frac{2\Omega_p\mathrm{Im}\rho_{13}^{(n)}}{\Gamma_{31}+\Gamma_{32}}, \tag{41}$$

$$\rho_{12}^{(n+1)}=-\frac{\Omega_p\left[D_2\Gamma\rho_{32}^{(n)}+2\Omega_c\left(\Omega_c\Gamma F_2^{(n)}-(D_2+2D_3)\mathrm{Im}\rho_{13}\right)\right]}{D_2\Gamma\left(\Delta_c+i\gamma_{12}\right)}, \tag{42}$$

$$\rho_{13}^{(n+1)}=\frac{i\Omega_p\left[\left(\rho_{11}^{(n)}-\rho_{33}^{(n)}\right)\left(D_1-\Omega_c^2\right)-iF_3^{(n)}\right]}{D_1\left(i\Delta_p-\gamma_{13}\right)}, \tag{43}$$

$$\rho_{23}^{(n+1)}=\frac{\Omega_p\left[\Omega_c\left(\rho_{11}^{(n)}-\rho_{33}^{(n)}\right)+iF_3^{(n)}\right]}{\Omega_c^2-\left(i\Delta_p-\gamma_{13}\right)\left(i\Delta_c-i\Delta_p+\gamma_{23}\right)}, \tag{44}$$

where:

$$D_1=\Omega_c^2-\left(i\Delta_p-\gamma_{13}\right)\left(i\Delta_c-i\Delta_p+\gamma_{23}\right), \tag{45}$$

$$D_2=\Delta_c^2\Gamma_{21}+\Gamma_{21}\gamma_{12}^2+4\Omega_c^2\gamma_{12}, \tag{46}$$

$$D_3=\Delta_c^2\Gamma_{32}+\Gamma_{32}\gamma_{12}^2-2\Omega_c^2\gamma_{12}, \tag{47}$$

$$\delta_1=i\Delta_c-\gamma_{12},\quad \delta_2=i\Delta_c+\gamma_{12},\quad \Gamma=\Gamma_{13}+\Gamma_{23}, \tag{48}$$

$$F_2^{(n)}=\rho_{23}^{(n)}\delta_1-\rho_{32}^{(n)}\delta_2, \tag{49}$$

$$F_3^{(n)}=\rho_{21}^{(n)}\left(i\Delta_p-\gamma_{13}\right). \tag{50}$$

2.3. Eigenfunctions and eigenenergies of the confined electron

The system we consider in this paper is the confined electron in a rectangular QD of sides L_1, L_2 and L_3. The Hamiltonian corresponding to this system can be written as:

$$H_0=-\frac{\hbar^2}{2m_e}\nabla^2+V(x,y,z), \tag{51}$$

where m_e is the effective electron mass. For GaAs quantum dot, the effective electron mass is $m_e = 0.067m_0$, where m_0 is the free electron mass. We choose the confining potential $V(x,y,z)$ to be equal to zero inside the box ($0 \le x \le L_1, 0 \le y \le L_2, 0 \le z \le L_3$) and infinite outside of the box. The time-independent Schrodinger equation that needs to be solved inside the box is:

$$-\frac{\hbar^2}{2m}\left(\frac{\partial^2}{\partial x^2}+\frac{\partial^2}{\partial y^2}+\frac{\partial^2}{\partial z^2}\right)\Psi(x,y,z) = E\Psi(x,y,z). \tag{52}$$

This equation is easily solved by separating variables and we found that eigenstates are standing waves:

$$\Psi_{n_1n_2n_3}(x,y,z) = \left(\frac{8}{L_1L_2L_3}\right)^{1/2}\sin\left(\frac{n_1\pi}{L_1}x\right)\sin\left(\frac{n_2\pi}{L_2}y\right)\sin\left(\frac{n_3\pi}{L_3}z\right), \tag{53}$$

where n_1, n_2 and n_3 are positive integers. Corresponding eingen energies are given by:

$$E_{n_3,n_2,n_1} = \frac{\hbar^2\pi^2}{2m}\left(\frac{n_1^2}{L_1^2}+\frac{n_2^2}{L_2^2}+\frac{n_3^2}{L_3^2}\right). \tag{54}$$

3. Results and Discussion

In this section, we investigate density matrix elements related to the confined electron in the rectangular QD. The system we consider is the three-level system forming the ladder and *V* configuration. The dynamics of these systems are described by master equations (11) - (15) and (30) - (34), respectively. The physical significance of matrix elements ρ_{21} for ladder configurations and ρ_{31} for *V* configurations consists in their relation to the susceptibility with respect to the probe field given by equations (Pavlović et al., 2016):

$$\chi = \frac{2N|d_{21}|}{\epsilon_0 E_p}\rho_{21} \qquad \text{for ladder configuration,} \tag{55}$$

$$\chi = \frac{2N|d_{31}|}{\epsilon_0 E_p}\rho_{31} \qquad \text{for } V\text{configuration,} \tag{56}$$

where *N* stands for the number density of the systems. By calculating the imaginary and real part of the susceptibility, we easily find the absorption and refraction index related to the probe field by using formulas (Pavlović et al., 2016):

$$\alpha = \frac{\omega}{c}\mathrm{Im}\chi\,, \tag{57}$$

$$n = \sqrt{1+\mathrm{Re}\chi}\,. \tag{58}$$

The existence of decay rates is the consequence of spontaneous emission and dephasing with its origin in the electron-phonon interaction. We denoted Γ_{21}, Γ_{32} and Γ_{31} to describe the spontaneous emission rates from state $|2\rangle$ to state $|1\rangle$, from state $|3\rangle$ to state $|2\rangle$ and from state $|3\rangle$ to state $|1\rangle$, respectively. At cryogenic temperatures (in the absence of the electron-phonon interaction), spontaneous emission dominates the relaxation mechanism and it is given by (Bransden et al., 2000):

$$\Gamma_{ij} = \frac{E_{ij}^3 |d_{ij}|^2}{3\pi\epsilon_0 \hbar^4 c^3}, \tag{59}$$

where E_{ij} denotes the energy difference between states $|j\rangle$ and $|i\rangle$. As it can be noted, the spontaneous emission depends on the dimension of the QD through dipole elements d_{ij} and energy differences E_{ij}. For higher temperatures (more than $7\,K$) the electron-phonon interaction can not be neglected. Thus, values for relaxation coefficients are experimentally determined and take values in a very broad domain - from $10^9 Hz$ to $10^{12} Hz$, see (Borri et al., 2001) and (Bayer et al., 2002).

3.1. Effect of quantum dot dimension on decay coefficients and eigenenergies

The quantum confinement of particles inside the QD leads to the discretization of energy levels. We obtained wave functions and corresponding eigenenergies for a confined electron in a rectangular QD given by (53) and (54). In the absence of an electromagnetic field, wave functions and corresponding eigenenergies of the confined electron in a rectangular QD are determined by three quantum numbers: n_1, n_2, and n_3. In order to implement the system of equations (11) - (15) to the system we consider, it is important to choose three states with the lowest eigenenergies.

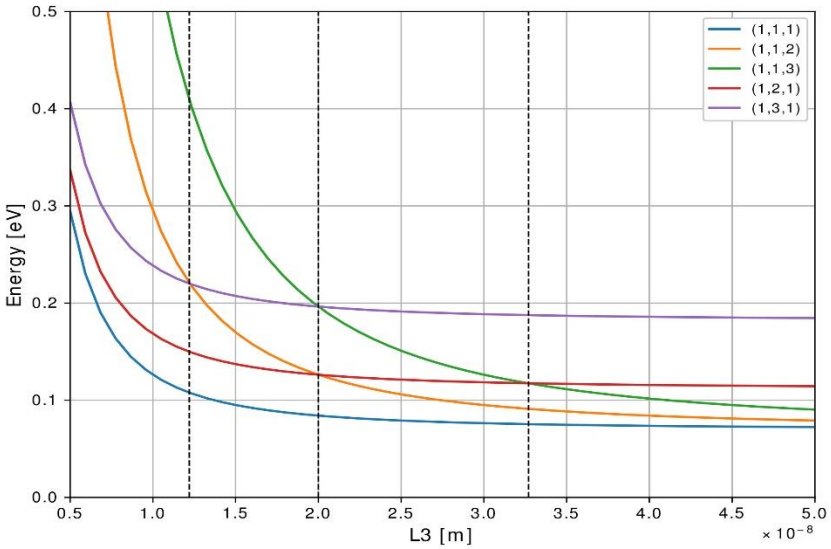

Fig. 2 Eigenenergies as functions of the QD dimension L_3 ($L_1 = 10.0$ nm and $L_2 = 20.0$ nm). It can be noticed that eigenenergies are inversely proportional to QDs dimensions, so the energy difference between any of the two states becomes smaller by increasing values of L_3.

The two sides of the rectangular QD are fixed: $L_1 = 10.0$ nm and $L_2 = 20.0$ nm. The third one - L_3, is varied from 5.00 nm to 50.0 nm. The dependence of eigenenergies on L_3 is depicted on Fig. 2. In this range of L_3 we can distinguish four domains (separated by dashed

lines on Fig. 2) with different eigenstates that correspond to the lowest eigenenergies. Three eigenstates represented by the tuple (n_1, n_2, n_3) with lowest eigenenegies in this domain are:

- (1,1,1); (1,2,1) and (1,3,1) for $L_3 \in$ [5.00 nm, 12.2 nm],
- (1,1,1); (1,2,1) and (1,1,2) for $L_3 \in$ [12.2 nm, 20.0 nm],
- (1,1,1); (1,1,2) and (1,2,1) for $L_3 \in$ [20.0 nm, 32.7 nm],
- (1,1,1); (1,1,2) and (1,1,3) for $L_3 \in$ [32.7 nm, 50.0 nm].

As we can notice, there are degenerate energy levels for certain values of L_3 in this domain. For $L_3 = 12.2$ nm states (1,3,1) and (1,1,2) correspond to the same eigenenergy as well as states (1,3,1) and (1,1,3), and (1,1,2) and (1,2,1) for $L_3 = 20.0$ nm and (1,1,3) and (1,2,1) for $L_3 = 32.7$ nm.

We also calculated decay rates due to spontaneous emission using formula (59) in order to find out what transitions are allowed among three states with the lowest energies. Their dependence on L_3 is represented on Fig. 3.

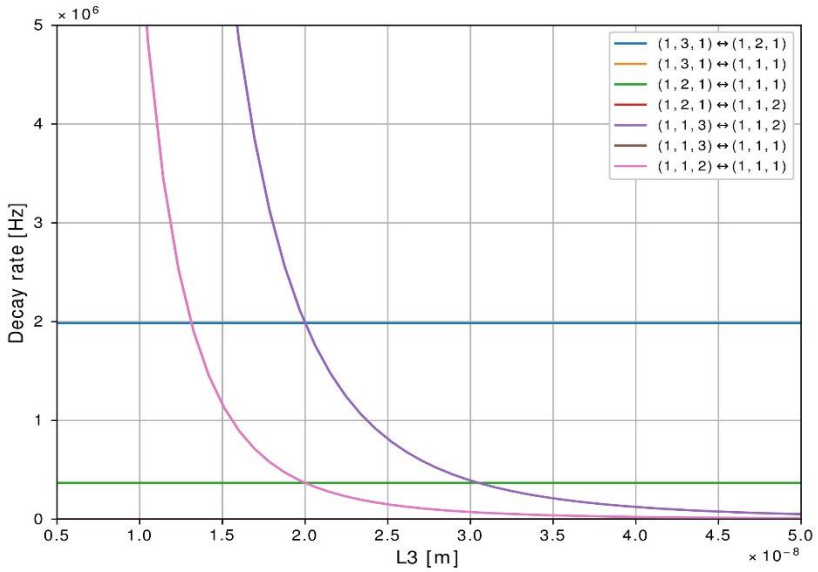

Fig. 3 Decay rates due to spontaneous emission for $L_1 = 10.0$ nm and $L_2 = 20.0$ nm as functions of L_3.

Since transitions (1,1,3) ↔ (1,1,1), (1,2,1) ↔ (1,1,2) and (1,3,1) ↔ (1,1,1) are dipole-forbidden, we can see that ladder configuration is formed in the first and in the fourth domain while *V* configuration is formed in the second and in the third domain depicted on Fig. 2.

3.2. Effect of quantum dot dimension on optical susceptibility

The optical susceptibility is connected to the density matrix elements via equations (55) - (56). The matrix element related to the susceptibility for ladder configuration (ρ_{21}) can be obtained from the system of equations (21) - (25). We concluded that for $L_3 >$ 32.7 nm three lowest energy states for a particle in a rectangular QD are identified by

quantum numbers (1,1,1), (1,1,2) and (1,1,3) and ladder configuration is formed among them. Assuming that the system is initially prepared in the ground state, we have that $\rho_{11}^{(0)} = 1$ and $\rho_{22}^{(0)} = \rho_{33}^{(0)} = \rho_{12}^{(0)} = \rho_{13}^{(0)} = \rho_{23}^{(0)} = 0$. Having these initial conditions $\rho_{21}^{(1)}$ can be obtained. For the term linear in Ω_p we obtain:

$$\rho_{21}^{(1)} = \frac{i\Omega_p}{\frac{\Omega_c^2}{(i\Delta_c + i\Delta_p + \gamma_{13})} + i\Delta_p + \gamma_{12}}. \tag{60}$$

The decay rate Γ_{31} is set to zero since the transition (1,1,3) ↔ (1,1,1) is dipole forbidden. Imaginary and real parts of $\rho_{21}^{(1)}$ as functions of the probe field detunings are plotted in a case of cryogenic temperatures. Thus, decay rates are calculated using equation (59). The electric fields of the control and probe lasers are both linearly polarized in the z direction with the intensity of 0.02 and 0.0002 V/m, respectively. In order to achieve the maximum effect, we also set detunings of the control field to be zero ($\Delta_c = 0$).

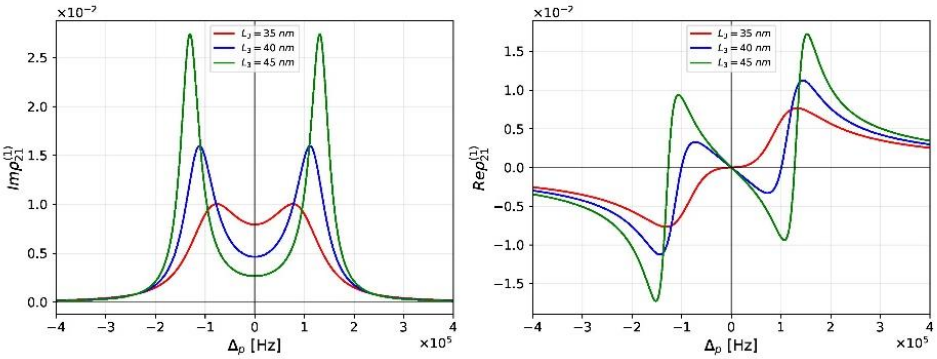

Fig. 4 Diagrams of the imaginary and real part of the matrix element $\boldsymbol{\rho_{21}^{(1)}}$ as the function of detunings of the probe laser field for different values of $\mathbf{L_3}$, and for $\mathbf{L_1 = 10.0}$ nm and $\mathbf{L_2 = 20.0}$ nm.

It can be seen from Fig. 4 that transparency windows have appeared for $L_3 = 40.0$ nm and $L_3 = 45.0$ nm and that values of $\mathrm{Im}\rho_{21}$ (proportional to the absorption coefficient) for zero detuning of the probe field decrease with the increase of the QD dimension.

From the system of equations (21) - (25) it can also be shown that the second and the fourth correction of the matrix element ρ_{12} ($\rho_{12}^{(2)}$ and $\rho_{12}^{(4)}$) are always equal to zero. In order to review the significance of the third and the fifth corrections of the matrix element ρ_{21}, they are plotted in Fig. 5. By comparing Fig. 4 and Fig. 5 we notice that corrections are decreasing in value up to two orders of magnitude. Thus, it is justified to take into account only the term linear in Ω_p since higher orders of corrections are negligible comparing to it.

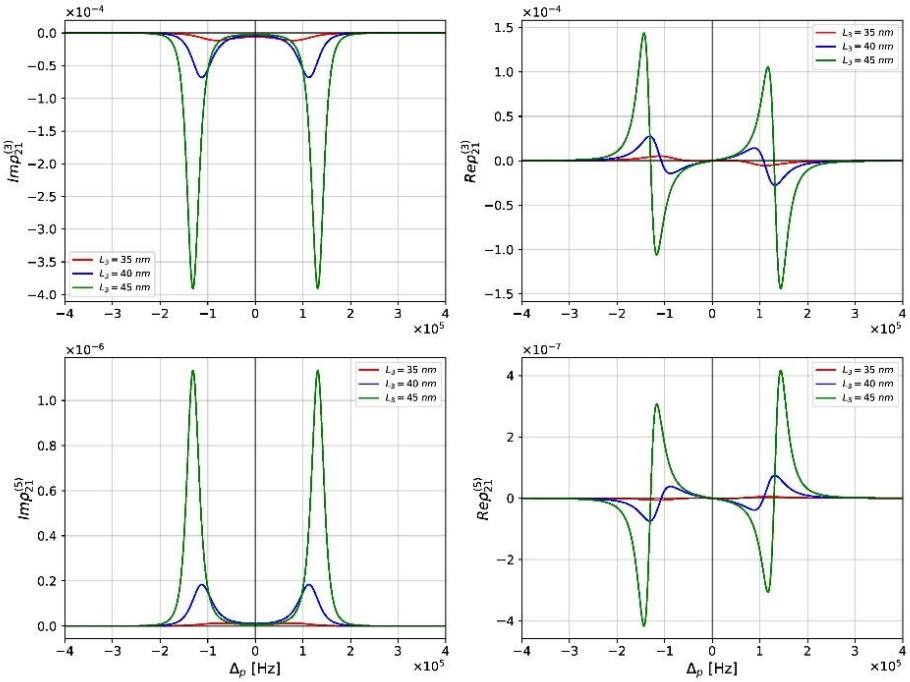

Fig. 5 The third and fifth correction of the imaginary and real part of the matrix element ρ_{21} as functions of probe field detunings, for $L_1 = 10.0$ nm, $L_2 = 20.0$ nm and several values of L_3.

Using the analog procedure for the *V* configuration and solving the system (35) - (39) in the steady-state regime we can obtain the expression for the matrix element $\rho_{31}^{(1)}$. The important difference compared to the ladder configuration is that now, the values of the matrix elements in the zeroth-order $\rho_{11}^{(0)}$, $\rho_{22}^{(0)}, \rho_{33}^{(0)}, \rho_{12}^{(0)}, \rho_{13}^{(0)}$ and $\rho_{23}^{(0)}$ are different. These matrix elements can also be calculated from the system (35) – (39) before we use their values to calculate these elements in the first order.

Now we set Γ_{32} to be equal to zero since we obtained that transition (1,1,2) ↔ (1,2,1) is dipole forbidden, for the third region in Fig. 2. Imaginary and real parts of $\rho_{31}^{(1)}$ as functions of the probe field detunings are plotted in Fig. 6. In order to obtain the EIT effect, the electric field of the control laser is polarized in the *z*-direction with the intensity of 0.2 V/m and probe laser is linearly polarized in the y direction with the intensity of 0.002 V/m.

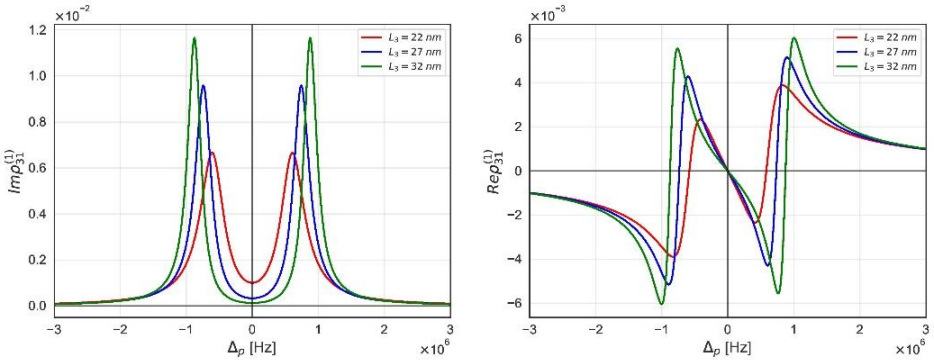

Fig. 6 Diagrams of imaginary and real parts of the matrix element $\rho_{31}^{(1)}$ for *V* configuration as the function of detunings of the probe laser field for $L_1 = 10.0$ nm, $L_2 = 20.0$ nm and several values of L_3.

It can be noted that transparency windows have appeared for all plotted values of L_3 for *V* configuration and transparency windows become wider by increasing the dimensions of QD.

3.3. Effect of dephasing rates on optical susceptibility

As it is mentioned earlier, at room or higher temperatures dephasing rates are significantly bigger than radiative decays and they cannot be neglected as in the case of cryogenic temperatures. For such temperatures, experimentally obtained values of decay rates are used. For the purpose of simplicity, we set decay rates $\gamma_{12} = \gamma_{13}$ for ladder and $\gamma_{13} = \gamma_{23}$ for *V* configuration. We found the dependence of imaginary and real parts of matrix elements ρ_{21} and ρ_{31} on probe field detunings for a constant value of L_3 and various values of decay rates. Electric fields of the probe and control lasers are increased 10^5 times but the same polarizations are used.

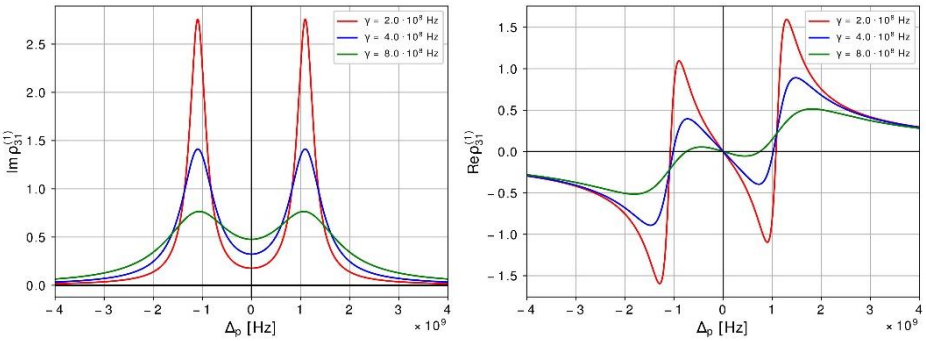

Fig. 7 The imaginary and real parts of $\boldsymbol{\rho_{21}^{(1)}}$ for constant dimensions of rectangular QD ($\mathbf{L_1 = 10}$ nm, $\mathbf{L_2 = 20}$ nm and $\mathbf{L_3 = 40}$ nm) and various values of decay coefficients $\boldsymbol{\gamma_{12} = \gamma_{13} = \gamma}$ as function of the probe field detunings for ladder configuration.

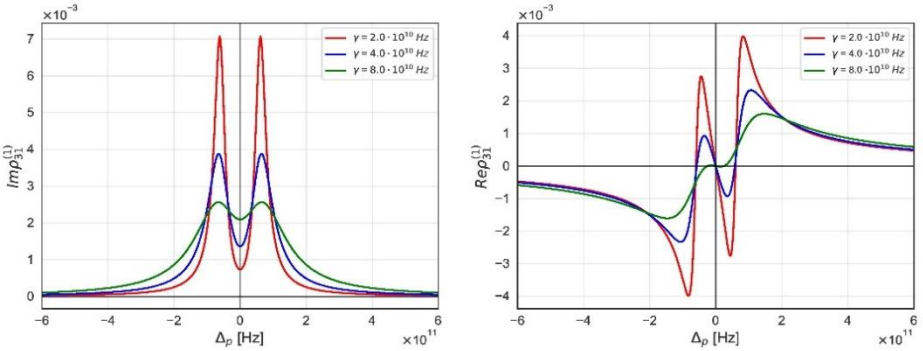

Fig. 8 Imaginary and real part of $\rho_{31}^{(1)}$ for constant dimensions of rectangular QD ($L_1 = 10$ nm, $L_2 = 20$ nm and $L_3 = 22$ nm) and various values of decay rates $\gamma_{13} = \gamma_{23} = \gamma$ as a function of the probe field detunings for V configuration.

A comparison of Fig. 7 to Fig. 4 and Fig. 8 to Fig. 6 leads to the conclusion that the qualitative properties of the transparency window and dispersion curve are the same. The quantitative difference is in the strengths of electric fields of lasers, which now need to be much higher, due to much larger losses. It can also be noticed that the minimum values of $\mathrm{Im}\rho_{21}^{(1)}$ for zero detuning increase, the peak values of $\mathrm{Im}\rho_{21}^{(1)}$ decrease, and peaks become wider, with the increase of decay rates values, which is in accordance with our previous work (Pavlović et al., 2016).

4. CONCLUSION

In this paper, we have studied EIT effect in the single electron semiconductor rectangular quantum dot of sides $L_1 = 10$ nm and $L_2 = 20$ nm, while the third side, L_3, is varied from 5 nm to 50 nm. The system we considered is the three-level system which is, depending on the concrete dimension of L_3, either in ladder or V configuration. In order to investigate the properties of this system we have written down master equations for each of these configurations and solved them for the steady-state regime using the perturbation method up to the fifth-order in Ω_p. Considering the fact that the even corrections for the ladder configuration are identically equal to zero and since it has been shown that the third-order and fifth-order corrections of matrix elements are negligible compared to the first, it is sufficient to consider only the first order of matrix elements of interest. Imaginary and real parts of matrix elements related to optical susceptibility are then plotted as functions of probe laser detunings. To summarize, we have concluded:

- By increasing QD dimensions, eigenenergies of the confined electron and spontaneous decay rates are decreased.
- In a case of ladder configuration, transparency windows are obtained for lasers polarized in z direction. By increasing dimension of L_3, the width of transparency windows is increased.
- Transparency windows are obtained for all plotted values of L_3 in a case of V configuration for the probe laser linearly polarized in y direction and the control laser

linearly polarized in z direction. Also, by increasing the dimension of the QD, the widths of transparency windows are increased.

- We also considered the EIT effect at room and higher temperatures for various values of decay rates whereby QD dimensions are set to constants. It has been noted that peaks appeared at the same positions for various values of decay rates, but the transparency window is diminished and completely vanished by increasing decay rates, for both ladder and V configurations.

REFERENCES

Arkhipkin, V. G., Heller, Yu. I., 1983. Phys. Lett. A, 98, 12. doi: 10.1016/0375-9601(83)90533-9
Bayer, M., Forchel, A., 2002. Phys. Rev. B 65, 041308(R). doi: 10.1103/PhysRevB.65.041308
Beausoleil, K. R., Munro, W. J., Rodrigues, D. A., Spiller T. P., 2004. J. Mod. Opt., 51, 16-18. doi: 10.1080/09500340408231802
Bing, Z., Yun, J., Gang, W., Li-Da, Z., Jin-Hui, W., Jin-Yue, G., 2011. Chin. Phys. B, 20, 050304. doi: 10.1088/1674-1056/20/5/050304
Boller, K. J., Imamoglu, A., Harris, S. E., 1991. Phys. Rev. Lett. 66, 2593-2596. doi: 10.1103/PhysRevLett.66.2593
Borri, P., Langbein, W., Schneider, S., Woggon, U., Sellin, R. L., Ouyang, D., Bimberg, D., 2001. Phys. Rev. Lett. 87, 157401. doi: 10.1103/PhysRevLett.87.157401
Bransden, B.H., Joachain, C.J., 2000. *Quantum Mechanic*, Pearson Education Edition, Harlow.
Budker, D., Kimball, D.F., Rochester, S.M., Yashchuk, V.V., 1999. Phys. Rev. Lett. 83(9), 1767-1770. doi: 10.1103/PhysRevLett.83.1767
Harris, S. E., 1989. Phys. Rev. Lett., 62(9), 1033-1036. doi:10.1103/PhysRevLett.62.1033
Hau, L.V., Harris, S.E., Dutton, Z., Behrooz, C.H., 1999. Nature 397, 594-598. doi:10.1038/17561
Kasapi, A., Maneesh, J., Yin, G. Y., Harris, S. E., 1995. Phys. Rev. Lett. 74(13), 2447-2450. doi:10.1103/PhysRevLett.74.2447
Kash, M.M., Sautenkov, V.A., Zibrov, A.S., Hollberg, L., Welch, G.R., Lukin, M.D., Rostovtsev, Y., Fry, E.S., Scully, M.O., 1999. Phys. Rev. Lett. 82(26), 5229-5232. doi:10.1103/PhysRevLett.82.5229
Liu, C., Dutton, Z., Behroozi, C.H., Hau, L.V., 2001. Nature 409, 490-493, (2001). doi:10.1038/35054017
Mirzaei, M., Askari, H.R., Raki, Z., 2014. Superlattices Microstruct. 74, 61-69. doi:10.1016/j.spmi.2014.06.011
pavlović, v., stevanović, lj., 2016. Superlattices Microstruct. 92, 10-23. doi:10.1016/j.spmi.2016.02.003
Wang, Z., 2009. Opt. Commun. 282(24), 4745-4748. doi:10.1016/j.optcom.2009.09.013

ELEKTROMAGNETNO INDUKOVANA TRANSPARENTNOST NA ELEKTRONU KONFINIRANOM KVANTNOM TAČKOM OBLIKA KVADRA

U ovom radu je proučavan efekat elektromagnetno indukovane transparentnosti (EIT) na elektronu zarobljenom unutar kvantne tačke (KT) oblika kvadra u prisustvu probnog i kontrolnog laserskog polja. Za realizaciju ovog efekta, izabrana su tri najniža energijska nivoa konfiniranog elektrona, koja u zavisnosti od dimenzija kvantne tačke mogu da čine kaskadnu ili V konfiguraciju. U radu je analizirana zavisnost elementa ρ_{21} matrice gustine za kaskadnu konfiguraciju i ρ_{31} za V konfiguraciju u zavisnosti od razdešenosti probnog polja za različite vrednosti dimenzija kvantne tačke. Ova zavisnost je ispitivana kako za kriogene temperature, pri kojima spontana emisija dominira nad relaksacionim mehanizmima, tako i za sobne temperature, kada se relaksacioni procesi ne mogu zanemariti.

Ključne reči: *Elektromagnetno indukovana transparentnost, Kvantna tačka, Kaskadna konfiguracija, Ve konfiguracija*